

CENTRAL ASIAN JOURNAL OF MEDICAL AND NATURAL SCIENCES
https://cajmns.casjournal.org/index.php/CAJMNS
Volume: 07 Issue: 04 | October 2026 ISSN: 2660-4159

Article

Green synthesis and Characterization of ZnO/Cr_2O_3 and ZnO/Cr_2O_3/Activated Carbon Nanocomposites Via Green Rout

Atallah Burjes Dakheel[1]

1. Department of Chemistry, College of Education for women, Tikrit University, Tikrit, Iraq
* Correspondence: atallah.b@tu.edu.iq

Abstract: The Green rout was used for the preparation of zinc oxide/chromium oxide (ZnO/Cr_2O_3) and ZnO/Cr_2O_3/Activated Carbon (AC) nanocomposites using the phytochemicals of Myrtus communis leaf extract as natural capping and reducing agents. The synthesized materials were subsequently characterized using scanning electron microscopy (SEM), energy-dispersive X-ray spectroscopy (EDX), Fourier-transform infrared spectroscopy (FTIR), and X-ray diffraction (XRD) to assess the effects of AC incorporation on the structures of materials, morphologies, and compositions. The results of SEM showed that the binary oxide composite morphology changed from rounded, densely agglomerated nanoparticles (49 nm) to angular, flake-supported morphology (61 nm) after the incorporation of AC. This compositional change was also quantified by EDX in which the binary oxide did not contain carbon whereas the AC containing composite did contain a significant carbon content (about 54.7 %). FTIR and XRD revealed that the characteristic Zn-O/Cr-O bonding as well as the crystalline framework of ZnO/Cr_2O_3 remained intact in both composites, and the broader hydroxyl absorption band along with the presence of an amorphous carbon diffraction feature (24° 2θ) also confirmed the successful incorporation of carbon. The results showed that the activated carbon can be embedded in a green synthesized ZnO/Cr_2O_3 without destroying its crystalline oxide structure and allow for the introduction of morphological and surface changes that may be relevant for the functional properties of the composite.

Keywords: Green Rout, Zinc Oxide, Chromium Oxide, Nanocomposites, Morphology

Citation: Dakheel. A. B. Green synthesis and Characterization of ZnO/Cr2O3 and ZnO/Cr2O3/Activated Carbon Nanocomposites Via Green Rout. Central Asian Journal of Medical and Natural Science 2026, 7(4), 854-865

Received: 13th Jul 2026
Revised: 28th Aug 2026
Accepted: 05th Sep 2026
Published: 16th Oct 2026

Copyright: © 2026 by the authors. Submitted for open access publication under the terms and conditions of the Creative Commons Attribution (CC BY) license (https://creativecommons.org/licenses/by/4.0/)

1. Introduction

Metal oxide (MO) nanoparticles demonstrate an essential position in the field of materials science and engineering due to their tunable thermal, optical, structural and catalytic characteristics [1] that used in a wide range of applications such as coating, gas sensing, inhibition agents, energy storage, and photocatalysis [2].

Among several types of metal oxides, chromium oxide (Cr_2O_3) is a thermally stable, chemically inert, commonly used for its antioxidant, antibacterial and corrosion and/or abrasion resistant properties, whereas zinc oxide (ZnO) is a semiconductor with a wide bandgap (about 3.3 eV) which is usually crystallizes in the structure of hexagonal wurtzite,

Common techniques used for synthesis of metal oxide nanoparticles are physical vapor deposition, co-precipitation, sol-gel route and hydrothermal process. However, these techniques are commonly relied on organic solvents, hazardous reducing agents, high energy inputs and/or an expensive instrumentation that raising concerns regarding cost, scalability and environmental safety. Green synthesis that exploits the capping and

reducing process of phytochemicals such as terpenoids, flavonoids, polyphenols and other metabolites found in extracts plant, has then arose as an decent alternative that works under suitable conditions, evades any toxic reagents, and produces particles in nano size with enhanced biocompatibility [3,4].

Myrtle (myrtus communis) is mediterranean plant with rich flavonoid and polyphenolic compounds that was previously used as a capping/reducing agent for the green rout of synthesizing ZnO nanoparticles. Sedefoglu shown that the morpholog, crystallinity, and photocatalytic characteristics of ZnO nanoparticles prepared with Myrtus communis extract via green rout can be modified through the type of selected zinc precursor and the temperature of calcination, with the samples showing the hexagonal wurtzite phase [5]. This indicated that the extract of myrtle leaves is an efficient biomaterial used for the green synthesis of zinc oxide nanoparticles.

In parallel, the green synthesis of Cr2O3 nanoparticles using other plant species, such as Abutilon indicum and Rhamnus virgata, also shows phytomolecules obtained from plants can serve as equal reducing and capping agents for chromium salts. This resulted in crystalline and biocompatible Cr2O3 nanoparticles with good antibacterial, antioxidant, and anticancer activity [6,7]. According to the published works in the current field, the extension of the green route involving Myrtus communis for synthesizing chromium oxide nanoparticles and the combination of green zinc oxide with chromium oxide to obtain a single calcined composite powder is not reported anywhere else.

The incorporation of two functional oxides into a single composite has proven to be a successful strategy to obtain properties that one constituent does not possess. Reports of related binary and ternary systems that combine ZnO with activated carbon (AC) show that surface area, adsorption capacity and electrochemical or photocatalytic performance can be better than the pure oxide [8,9].

The biomass-derived activated carbons are green precursors with interesting characteristics. Indeed, it has been shown by Megherbi et al. [10] that Myrtus communis leaves can be converted into activated carbon with a well-developed porous structure by way of H_3PO_4 chemical activation. Moreover, the specific surface area significantly increases with the H_3PO_4 impregnation ratio. This finding indicates that metal oxide precursors and carbon additive of a single composite formulation can derive from one common, low-cost and locally available biomass source Myrtus communis leaves.

Nanostructured oxide and oxide/carbon composites are also of practical interest for the surface protection of metallic substrates. Green synthesized nanoparticles and nanocomposites have been increasingly examined as green corrosion resistance coating additives and inhibitors for steel and stainless steel [11]. In light of the above, the present study intends to: (i) green synthesize ZnO and Cr_2O_3 NPs separately using the leaf extract of Myrtus communis (M. communis) for reducing and capping of both oxides in an aqua medium. (ii) First, collect myrtle leaves and treat them with heat and acid and then mix two green oxide powders in equal proportions and heat the mixture to obtain a binary Nano ZnO-Cr2O3 nanocomposite (Sample 1). (iii) Lastly, an activated carbon from the same myrtle leaves will be prepared through carbonization and phosphoric acid activation; which then be mixed into the ZnO-Cr2O3 mixture before heating to obtain a ternary Nano ZnO-Cr2O3 / AC nanocomposite (Sample 2) Analytical characterization will then be undertaken to evaluate the phase composition, morphology and functional chemistry of the composite powders.

2. Materials and Methods

2.1 Chemicals and Materials

The leaves of the plant Myrtus communis (Myrtle) were used as the only botanical source for the synthesis of the nanoparticles and for the activated-carbon precursor. As solvents, distilled water and absolute ethanol were used. The zinc precursor was zinc nitrate hexahydrate ($Zn(NO_3)_2{\cdot}6H_2O$) or zinc acetate dihydrate ($Zn(CH_3COO)_2{\cdot}2H_2O$) and the chromium precursor was chromium(III) nitrate nonahydrate ($Cr(NO_3)_3{\cdot}9H_2O$). As precipitant, sodium hydroxide (NaOH) was used, when it was required, and as a chemical activating agent for the preparation of activated carbon, orthophosphoric acid (H3PO4, 85

wt.%) was used. The reagents were all analytical grade and were used as received, and distilled water was used to prepare all aqueous solutions.

2.2 Leaf extract preparation

The extraction of aqueous Myrtus communis leaf extract was performed by the following steps: The surface dust and debris were removed from healthy myrtle leaves by washing them with tap water and then distilled water before shade-drying at room temperature in the shade. The dried leaves were milled in a laboratory mill to a fine powder. Known mass of leaf powder was transferred to distilled water (and where indicated, aqueous ethanol) and heated while stirring continuously for approximately one hour at about 80 ± 5 °C to extract any soluble phytochemicals. This extract was then cooled to room temperature, filtered through Whatman No. 1 filter paper to remove the particulate residue and kept at 4 °C until needed.

2.3 ZnO nanoparticles synthesis

A fixed mass of $Zn(NO_3)_2{\cdot}6H_2O$ (or zinc acetate) was dissolved in distilled water to prepare the zinc precursor solution. The leaf extract of Myrtus communis was dropped into the precursor solution while continuously stirring with magnetic stirrer at room temperature (or under mild heating conditions). The emergence of visible color change of the reaction mixture and the gradual formation of a light precipitate suggested the beginning of the formation of ZnO nanoparticles, promoted by the reducing and capping properties of phytochemicals present in the extract. The mixture was stirred again for an additional time to ensure the reaction was complete, and then the precipitate was centrifuged, washed many times with both distilled water and ethanol, to remove any remaining unreacted precursor and organics, and dried in an oven. The dried powder was then calcined in a muffle furnace at 400 °C for 30 minutes to remove any trace of organic material and to facilitate the crystallization of the hexagonal wurtzite ZnO structure, as required by the reported synthesis method of ZnO by Myrtus communis [1].

2.4 Cr_2O_3 nanoparticles synthesis

Cr_2O_3 nanoparticles were also synthesized according to a similar plant-mediated method. The extraction solution of Myrtus communis leaves was added dropwise to an aqueous solution of $Cr(NO_3)_3{\cdot}9H_2O$ while being stirred. The formation of the precursor phase Cr_2O_3 was visually detected in the reaction mixture by the characteristic color change of the reaction mixture, which corresponds to the reduction and capping of the ions Cr^{3+} by the phytomolecules of the extract, as reported in other plant-mediated Cr_2O_3 synthesis [2,3]. The precipitate was collected by centrifuging, washed with distilled water and ethanol, dried and calcined to form the crystalline nanopowder of Cr_2O_3.

2.5 Activated carbon Synthesis

The activated carbon was prepared from Myrtus communis leaves using the following method.The activated carbon was prepared from Myrtus communis leaves with the following method: The same source of myrtle leaves was used to produce the activated carbon following a chemical activation route similar to that described for the production of the activated carbon from phosphoric-acid activated Myrtus communis leaves [4]. Controlled heating of dried, powdered myrtle leaves to char the wood was the first step in the method. The char was then impregnated with orthophosphoric acid (H_3PO_4) at a desired impregnation ratio and allowed to equilibrate prior to activation in a furnace at around 450 °C for about 1 hour. The activated product was repeatedly washed with hot distilled water to neutralize the wash water (removal of the residual phosphoric acid and soluble ash), and then dried and ground to fine powder to make the activated carbon (AC) for the ternary composite formulation from myrtle-leaf.

2.6 ZnO/Cr_2O_3 nanocomposite preparation

Calcined ZnO/Cr_2O_3 nanocomposite (sample 1) was prepared via mixing the ZnO and Cr_2O_3 as per the optimized parameters and a calcination process was performed at 400 °C for 60 minutes. The green synthesized powder of ZnO and Cr_2O_3 were weighed and mixed in 1:1 ratio. Dry grinding in an agate mortar (and/or brief ball-milling) was used to ensure

intimate mixing of the two oxide phases. The homogenized powder mixture was then placed in an alumina crucible and calcined in a controlled heating profile in a muffle furnace to give the final binary ZnO/Cr_2O_3 nanocomposite powder, which is designated as Sample 1.

2.7 ZnO/Cr_2O_3/AC preparation

Sample 2 (ZnO/Cr_2O_3/AC) ternary composite was synthesized by calcination the mixture of ZnO and activated carbon (AC) at 400 °C for 60 minutes. The similar blend (1:1 (by mass) ZnO/Cr_2O_3 as used in Section 2.6 was used for Sample 2, with the addition of a defined mass fraction of the activated carbon derived from Myrtus communis (described in Section 2.5) before homogenization. Dry grinding was used to homogenize the ternary powder mixture, which was then calcined in the same manner as Sample 1 to prepare the final ZnO/Cr_2O_3/AC ternary nanocomposite. The calcination temperature, heating rate, and dwell time for Sample 2 were selected with special consideration for the need to maintain an acceptable carbon level after the activated carbon is oxidized and has burned away at the elevated temperature in air.

2.8 Characterization

These two composite powders (Samples 1 and 2) were analysed with a set of analysis techniques which also includes the individual green-synthesized ZnO, Cr_2O_3, and activated-carbon powders. Using the X-ray diffraction (XRD) technique, the crystalline phases present was identified, and the average crystallite size was estimated using the Debye–Scherrer equation, which is also applicable to the wurtzite form of ZnO and the eskolaite form of Cr_2O_3. The identification of metal/oxygen vibrational bands and the existence of residual surface functional groups from the plant extract and the activated carbon was determined using Fourier transform infrared spectroscopy (FTIR) while the morphology, agglomeration state and elemental composition of particles was analyzed by scanning electron microscopy (SEM) and energy-dispersive X-ray spectroscopy (EDX).

3. Results

3.1.1 SEM

The morphological properties of the nanocomposites, ZnO/Cr_2O_3 (sample 1) and ZnO/Cr_2O_3/AC (sample 2) were studied and compared at two different magnification (low 4000x and high 120,000x) via SEM (Fig. 1 and Figure 3 respectively). The Sample 1 at low magnification shows an agglomerated texture with relatively homogeneous porosity and rounded, coalesced clusters, resembling a cauliflower. Sample 2 on the other hand shows a more heterogeneous and fragmented architecture of the ZnO/Cr_2O_3 matrix containing finer particulate matter and angular and plate-like fragments, which can be interpreted as the presence of activated carbon (AC) in the matrix. The AC component, which is also produced from a different precursor and carbonization process, is morphologically different from the oxide nanoparticles and is characterized by sheet-like / flaky pieces having sharp edges and flat facets, resulting in the Sample 2 having a more irregular and rougher low magnification texture than Sample 1.

This difference is more pronounced at high magnification. The quasi-spherical nanoparticles of sample 1 have surfaces with smooth, rounded and cauliflower-like texture, with a mean diameter of approximately 49 nm, and a size range of 44.65-53.04 nm. In contrast, the high-magnification micrograph of Sample 2 shows mostly angular, plate-like particles with sharp facet boundaries of 46.59–77.14 nm (mean ≈ 61 nm), which are larger than Sample 1, both in terms of mean size and width of size distribution. This is in line with two mechanisms: (i) the surrounding of the carbon flakes by the already nucleated and growing ZnO/Cr_2O_3 should be non-uniform, allowing for a larger and more polydisperse particle size, and (ii) partial masking/overlap of the oxide nanoparticles by the underlying carbon flakes can lead to overestimated particle size in the SEM projection [12].

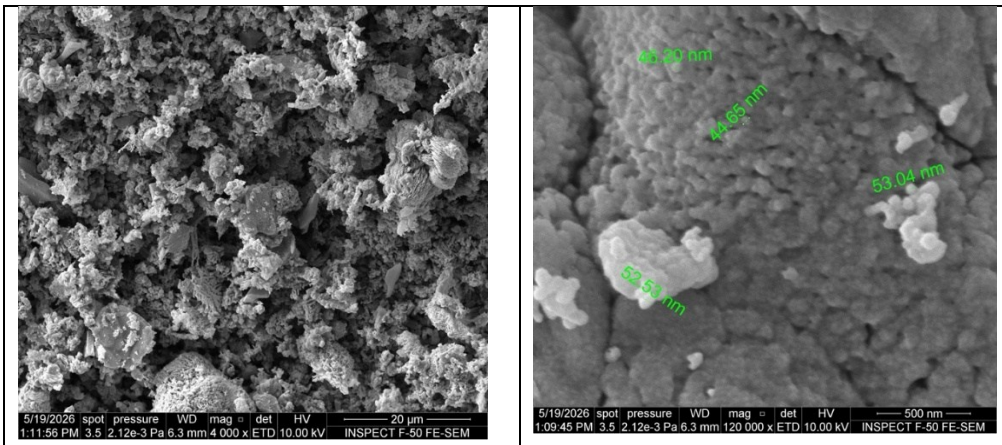
Comparative SEM analysis generally shows that the incorporation of AC affects the composite assembly (from Sample 1: homogeneous, rounded nanoparticle agglomerate, to Sample 2: heterogeneous, larger grain, flake-supported), which will be expected to impact surface area, active-site accessibility, and therefore the functional performance of the composite (such as adsorption/photocatalytic behavior).

3.1.2 EDX

The quantitative EDX analysis shows that there is a basic compositional difference between the two nanocomposites. Sample 1 (ZnO/Cr_2O_3) is dominated by zinc (86.4 at%, 88.8 wt%) with chromium present as a minor constituent (13.6 at%, 11.2 wt%), giving a Zn:Cr atomic ratio of ≈ 6.4:1 (Figure 2). The amount of carbon signal was not quantified for this sample, as the sample was formulated as a binary oxide composite.

Sample 2 (ZnO/Cr_2O_3/AC), however, presents a significant amount of carbon, with the total being 54.7 at% (19.4 wt%), providing direct, quantitative evidence of successful addition of activated carbon to the composite matrix (Figure 4). This large carbon fraction reduces the relative oxide proportion in the composition as follows: the atomic ratio of Zn/Cr changes to approximately 1.8:1 (the atomic ratio of Zn/oxide changes to approximately 2.6:1), with a reduction in the atomic proportion of zinc (55.6 wt% oxide) and an increase in the atomic proportion of chromium (25.1 wt% oxide). This increased relative Cr and decreased relative Zn signal (compared to Sample 1) is best understood as due to dilution by the carbon because it has such a large contribution to the interaction volume sampled by the electron beam and not as an actual change in the underlying Zn:Cr ratio of the oxide phase itself [13].

In combination with the SEM morphology (angular particles supported by flakes in Sample 2 and rounded oxide agglomerates in Sample 1), the EDX data support the fact that the activated carbon is not a simple physical addition, but a intimately integrated part of the composite architecture, in agreement with the SEM observation of oxide nanoparticles decorating the surfaces of the carbon flakes.



(a) (b)

Figure 1. SEM of ZnO/Cr_2O_3 nanocomposite (sample 1)

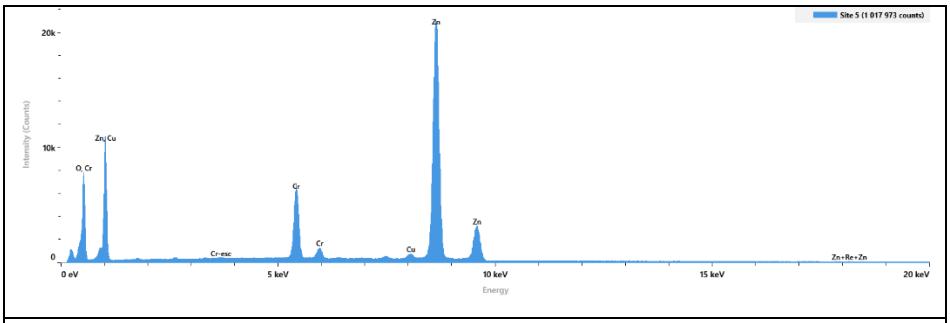
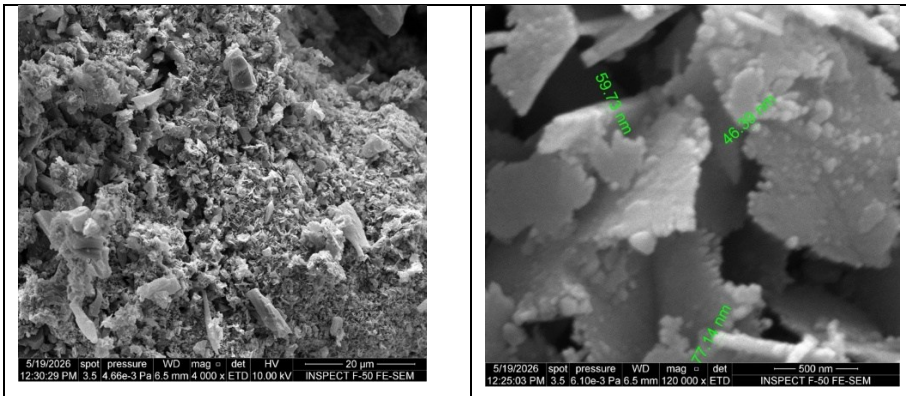


Figure 2. EDX of ZnO/Cr_2O_3 nanocomposite (sample 1)



(a) (b)

Figure 3. SEM of ZnO/Cr_2O_3/Activated carbon nanocomposite (sample 2)

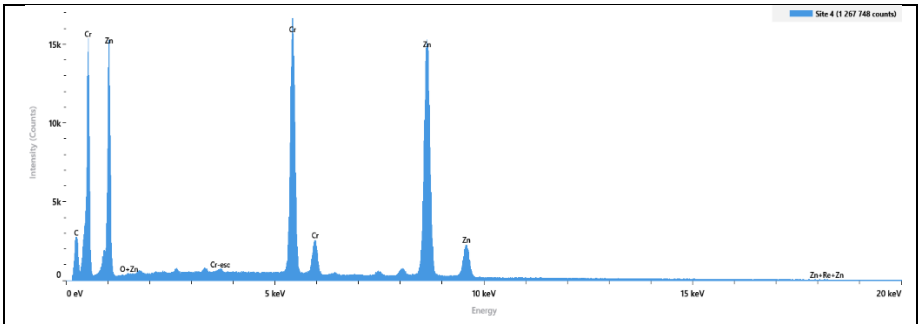


Figure 4. EDX of ZnO/Cr_2O_3/Activated carbon nanocomposite (sample 2)

3.2 Structure

3.2.1 FTIR

The identification of the functional groups and metal-oxygen bonding in the two nanocomposites (Fig. 5 and 6) was achieved using FTIR spectroscopy. Both samples have shown a wide band of absorption at 3300-3550 cm^{-1}, which corresponds to O-H stretching vibrations of surface adsorbed water and hydroxyl groups, as well as the phenolic O-H, which could be due to the residual functional group from the synthesis with the aid of an extract from the Myrtus communis leaf. The band's width and position are shifted slightly to higher wave numbers in Sample 2 (3506.6, 3444.9, 3360.0 cm^{-1}) than in Sample 1 (3448.7, 3388.9 cm^{-1}), which is consistent with the other oxygen-containing surface functionalities (hydroxyl groups, carboxylic groups), which are usually added to activated carbon.

The bands in the middle range of the spectra (at 1620-1650 cm^{-1}), which appear in both, are assigned to H-O-H bending of the adsorbed water and to the C=C stretching of the

aromatic rings of the residual plant phytoconstituents and, in Sample 2, of the AC framework itself. The bands at 1460-1296 cm^{-1} (observed in both samples, but close to each other e.g., 1383.0 and 1296.2 cm^{-1}) are attributed to C-H bending and carboxylate (COO^-) stretching, and may be interpreted as indicative of organic surface residues in both composites, although in general this region is more intense and diagnostic for activated-carbon-containing materials due to aromatic and carboxyl functionalities derived from the lignin.

The presence of C-O stretching vibration is assigned to the bands at nearly the same position (1180-1115 cm^{-1}) in both samples, and thus the position of this functional group remains unchanged even after incorporating AC.

The region of the spectra (on 655.8 cm^{-1} for Sample 1, about 432 cm^{-1} for Sample 1 and about 444 cm^{-1} for Sample 2), is the most diagnostic for the presence of Zn-O and Cr-O lattice (metal–oxygen) stretching vibrations [14,15]. The appearance of this band in both samples supports the idea that the AC incorporation does not significantly disrupt the ZnO/Cr_2O_3 oxide framework, with the nearly identical position between the samples (432 and 444 cm^{-1}) indicating that the local metal-oxygen bonding environment is not significantly disrupted by AC incorporation.

Overall, the FTIR results support the two complementary conclusions mentioned above: (i) the core Zn-O/Cr-O oxide bonding signature remains unchanged for both samples, indicating successful formation of the metal oxide phase in both cases and confirming that the additional oxygenated/aromatic surface chemistry introduced by the activated carbon is not interfering with the oxide phase; and (ii) the hydroxyl region is broadened for Sample 2, and the relative intensities of the organic functional group bands are comparable to-similar relative to the intensity of the oxygen bonding band (confirming the quantitatively strong carbon signal was detected by the EDX analysis.

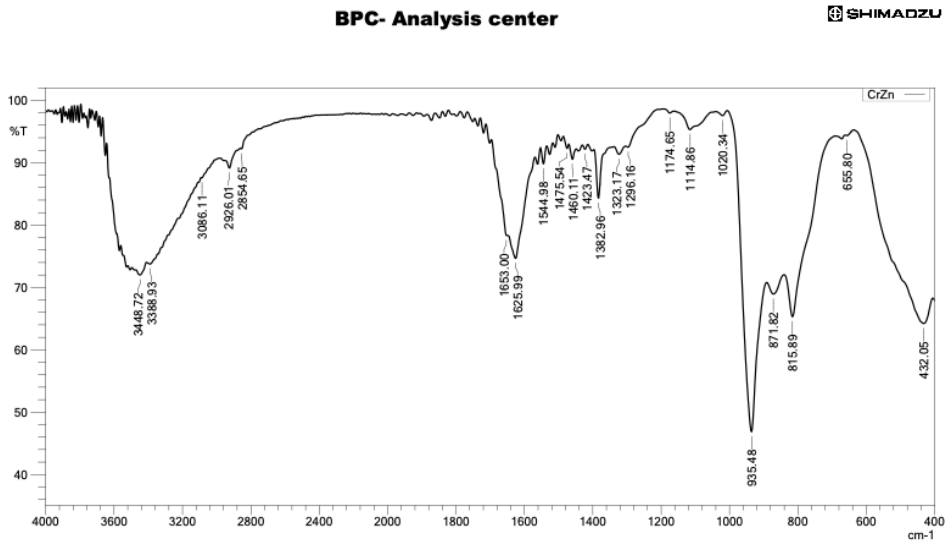


Figure 5. FTIR of ZnO/Cr_2O_3 nanocomposite (sample 1)

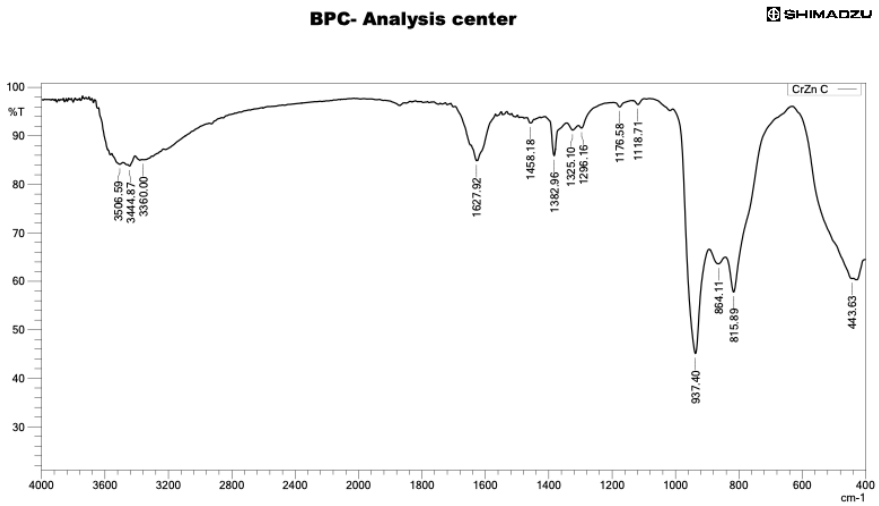


Figure 6. FTIR of ZnO/Cr_2O_3/Activated carbon nanocomposite (sample 2)

3.2.2 XRD

The XRD patterns of both nanocomposites (Fig. 7–8) show a similar series of diffraction peaks that are centered within the same 2θ angle range (25–90°), and positions of the peaks in Sample 2 are compared with Sample 1 and are within ~0.1° of each other at each corresponding peak [5]. The crystallinity of both composites remains unaffected from the peak alignment and the same crystalline oxide phases, compatible with ZnO (wurtzite) and Cr_2O_3 (rhombohedral) are present in both composites. However, the presence of well-resolved reflections in both patterns further confirms that the ZnO–Cr_2O_3 phase is well-crystallized in both types of carbon support.

The most striking difference between the two patterns is the presence of an extra wide feature at around 24° 2θ in Sample 2 which is not (or is not significantly) present in Sample 1. The broad hump in this region is typical of the (002) reflection of amorphous or turbostratic carbon, which may be found in many activated-carbon-containing materials, as their stacking is damaged. The presence of this feature only in sample 2 is also consistent with and supports the high carbon content already quantifiably confirmed by EDX (54.7 at% C) and qualitatively confirmed by the broadened organic/hydroxyl bands in the FTIR spectrum of the same sample.

The XRD results, when considered together with the results obtained from the SEM, EDX and FTIR analyses already discussed, fully support two conclusions: (a) the crystalline framework of the ZnO–Cr_2O_3 oxides is well formed and preserved in both samples and (b) the presence of an amorphous carbon phase is only evident in the XRD result for Sample 2, thus demonstrating successful, structurally unique incorporation of activated carbon into the composite.

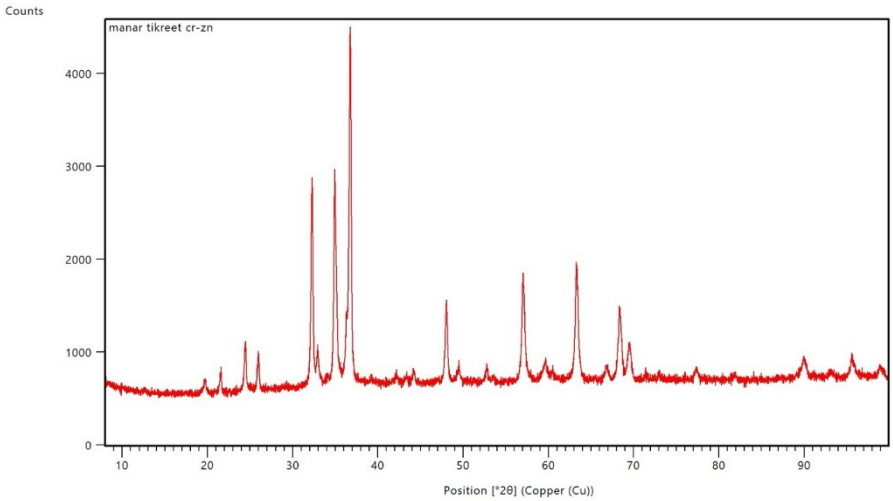


Figure 7. XRD of ZnO/Cr_2O_3 nanocomposite (sample 1)

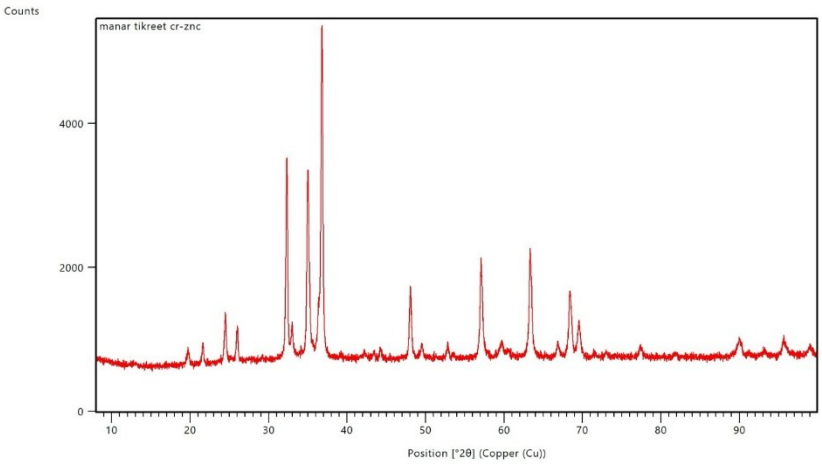


Figure 8. XRD of ZnO/Cr_2O_3/Activated carbon nanocomposite (sample 2)

4. Discussion

The present findings demonstrate that the incorporation of activated carbon (AC) into the green-synthesized ZnO/Cr_2O_3 system substantially modifies the morphological and surface characteristics of the nanocomposite while preserving the fundamental crystalline structure of the metal oxides. SEM observations revealed a clear transition from the relatively homogeneous, rounded, and densely agglomerated morphology of ZnO/Cr_2O_3 to a more heterogeneous architecture consisting of angular and plate-like particles supported by carbonaceous flakes in ZnO/Cr_2O_3/AC. The increase in the mean particle size from approximately 49 nm to 61 nm further indicates that AC influences particle assembly and aggregation during composite formation. Such morphological modification may result from the deposition and growth of oxide nanoparticles on the irregular surface of activated carbon, which provides additional interfaces for particle attachment. The broader particle-size distribution observed in the ternary composite may also be associated with the overlap of oxide particles with carbon flakes during SEM measurement. Similar morphological effects have been reported in green-synthesized nanomaterials, where interactions between inorganic nanoparticles and supporting phases influence particle growth and final surface architecture [12]. Therefore, the SEM findings suggest that AC functions not merely as an additive but as a structural component that reorganizes the ZnO/Cr_2O_3 composite architecture.

The EDX results provide further evidence supporting the successful incorporation of activated carbon into the ternary nanocomposite. The ZnO/Cr_2O_3 sample was predominantly composed of zinc and chromium, whereas the ZnO/Cr_2O_3/AC composite exhibited a substantial carbon content of approximately 54.7 at%. This compositional difference corresponds well with the flake-supported structures observed in the SEM images and confirms the presence of a carbon-rich phase within Sample 2. The apparent alteration in the relative Zn and Cr signals after AC incorporation should not necessarily be interpreted as a fundamental modification of the original oxide stoichiometry because EDX measures the elemental composition within a localized electron-beam interaction volume. Instead, the strong carbon contribution can dilute the relative signals originating from the metal oxide phases. This interpretation is consistent with the heterogeneous distribution of oxide particles over carbonaceous structures observed microscopically. Consequently, the complementary SEM and EDX results indicate that activated carbon is effectively integrated within the ZnO/Cr_2O_3 matrix rather than existing solely as a physically separated component.

The FTIR analysis further clarifies the chemical interactions occurring within the synthesized composites. Both samples exhibited characteristic absorption features associated with hydroxyl groups, residual organic functionalities, and metal–oxygen vibrations. Importantly, the persistence of the Zn–O and Cr–O vibration region in both composites demonstrates that incorporation of activated carbon does not substantially disrupt the fundamental metal–oxygen bonding environment. The broader hydroxyl absorption observed in the AC-containing composite can reasonably be associated with additional oxygen-containing surface groups contributed by activated carbon, including hydroxyl and carboxylic functionalities. These groups may originate from both the biomass precursor and the phosphoric-acid activation process used to prepare the carbon material. At the same time, the preservation of characteristic metal–oxygen bands indicates that the oxide components remain structurally distinguishable after formation of the ternary system. The FTIR findings therefore demonstrate coexistence between the inorganic ZnO/Cr_2O_3 framework and the oxygenated surface chemistry associated with activated carbon rather than extensive chemical destruction or transformation of the oxide phases. This coexistence is particularly important because surface functional groups can potentially provide additional interaction sites while the intrinsic structural characteristics of ZnO and Cr_2O_3 are maintained.

The XRD results reinforce this interpretation by demonstrating that both composites retain well-defined crystalline oxide phases attributable to ZnO and Cr_2O_3. The close correspondence between the diffraction peak positions of Samples 1 and 2 indicates that the addition of activated carbon does not cause substantial structural alteration of the ZnO/Cr_2O_3 crystalline framework. The most distinctive feature of the ternary composite is the broad diffraction contribution around 24° 2θ, which is consistent with the presence of an amorphous or turbostratic carbon phase. This observation agrees with the strong carbon signal detected by EDX and the enhanced organic and hydroxyl characteristics identified by FTIR. Thus, XRD, FTIR, EDX, and SEM provide mutually supportive evidence for successful formation of the ZnO/Cr_2O_3/AC composite. Rather than replacing or destroying the crystalline oxide phases, the activated carbon appears to coexist with and support these phases within a heterogeneous composite architecture. The preservation of oxide crystallinity is important because the structural properties associated with ZnO and Cr_2O_3 can potentially be retained while additional surface characteristics are introduced through the carbon phase.

Taken together, the characterization results demonstrate that the green synthesis route using *Myrtus communis* provides a viable strategy for producing both binary ZnO/Cr_2O_3 and ternary ZnO/Cr_2O_3/AC nanocomposites. An important aspect of this approach is that the same botanical source contributes to the synthesis of the metal oxide nanoparticles and serves as the precursor for activated carbon, providing a more

integrated biomass-based preparation route. Previous research has demonstrated the suitability of *Myrtus communis* extract for green ZnO synthesis [5], while activated carbon prepared from *Myrtus communis* leaves has also been reported to possess useful porous and surface characteristics [10]. The present study extends these approaches by integrating the oxide and carbon components into a single ternary material. The resulting composite combines preserved ZnO/Cr_2O_3 crystallinity with a carbon-rich, morphologically heterogeneous surface. Such structural characteristics may potentially improve surface interaction, adsorption, active-site accessibility, and interfacial processes compared with the binary oxide system. Nevertheless, these functional advantages should be regarded as prospective because the present study primarily establishes structural, morphological, and compositional characteristics rather than directly measuring adsorption, photocatalytic, electrochemical, or corrosion-protection performance. Future studies should therefore correlate these characterization results with specific functional tests to determine whether the observed structural modifications translate into measurable improvements in material performance.

5. Conclusion

The SEM, EDX, FTIR and XRD analyses of the synthesized Sample 1 (ZnO/Cr_2O_3) and Sample 2 (ZnO/Cr_2O_3/AC) nanocomposites were performed. The results of SEM revealed that in Sample 1 nanoparticles were rounded and agglomerated while in Sample 2, they were larger, angular with flake support. EDX confirmed this structural change to be compositional: Sample 2 contained a significant signal of carbon (54.7 at%) which was not present in Sample 1, thus confirming successful incorporation of AC. The results of FTIR and XRD confirmed that the core Zn-O/Cr-O bonding and ZnO/Cr_2O_3 crystalline framework has remained intact for both the samples; Sample 2 further exhibited a broader hydroxyl FTIR band and a clear amorphous-carbon XRD reflection (~24° 2θ) verifying the EDX analysis. These results together demonstrate the successful incorporation of activated carbon into the composite, no apparent disruption of the underlying oxide material, and that the carbon surface and morphology likely will affect the functional performance of the material.

REFERENCES

[1] U. Farooq, T. Ahmad, F. Naaz, and S. U. Islam, "Review on metals and metal oxides in sustainable energy production: Progress and perspectives," Energy & Fuels, vol. 37, no. 3, pp. 1577–1632, 2023.

[2] M. S. S. Danish, A. Bhattacharya, D. Stepanova, A. Mikhaylov, M. L. Grilli, M. Khosravy, and T. Senjyu, "A systematic review of metal oxide applications for energy and environmental sustainability," Metals, vol. 10, no. 12, Art. no. 1604, 2020.

[3] A. M. E. Shafey, "Green synthesis of metal and metal oxide nanoparticles from plant leaf extracts and their applications: A review," Green Processing and Synthesis, vol. 9, no. 1, pp. 304–339, 2020.

[4] P. C. Nagajyothi, S. V. Prabhakar Vattikuti, K. C. Devarayapalli, K. Yoo, J. Shim, and T. V. M. Sreekanth, "Green synthesis: Photocatalytic degradation of textile dyes using metal and metal oxide nanoparticles—Latest trends and advancements," Critical Reviews in Environmental Science and Technology, vol. 50, no. 24, pp. 2617–2723, 2020.

[5] N. Sedefoglu, "Green synthesis of ZnO nanoparticles by Myrtus communis plant extract with investigation of effect of precursor, calcination temperature and study of photocatalytic performance," Ceramics International, vol. 50, no. 6, pp. 9884–9895, 2024.

[6] S. A. Khan, S. Shahid, S. Hanif, H. S. Almoallim, S. A. Alharbi, and H. Sellami, "Green synthesis of chromium oxide nanoparticles for antibacterial, antioxidant, anticancer, and biocompatibility activities," International Journal of Molecular Sciences, vol. 22, no. 2, Art. no. 502, 2021.

[7] J. Iqbal, B. A. Abbasi, A. Munir, S. Uddin, S. Kanwal, and T. Mahmood, "Facile green synthesis approach for the production of chromium oxide nanoparticles and their different in vitro biological activities," Microscopy Research and Technique, vol. 83, no. 6, pp. 706–719, 2020.

[8] B. Y. Mekonnen, D. A. Fentaw, and M. A. Zeleke, "Synthesis and characterization of ZnO/activated carbon khat nanocomposite for removal of methylene blue dye," Indian Journal of Chemical Technology, vol. 31, no. 3, pp. 462–469, 2024.

[9] I. M. Mohamed, A. S. Yasin, and C. Liu, "Synthesis, surface characterization and electrochemical performance of ZnO@ activated carbon as a supercapacitor electrode material in acidic and alkaline electrolytes," Ceramics International, vol. 46, no. 3, pp. 3912–3920, 2020.

[10] H. Megherbi, H. Runtti, S. Tuomikoski, A. Heponiemi, T. Hu, U. Lassi, and A. Reffas, "The effect of phosphoric acid on the properties of activated carbons made from Myrtus communis leaves: Textural characteristics, surface chemistry, and capacity to adsorb methyl orange," Journal of Molecular Structure, vol. 1321, Art. no. 140038, 2025.

[11] S. Yadav, A. P. Raman, M. B. Singh, I. Massey, P. Singh, C. Verma, and A. AlFantazi, "Green nanoparticles for advanced corrosion protection: Current perspectives and future prospects," Applied Surface Science Advances, vol. 21, Art. no. 100605, 2024.

[12] V. Selvanathan, M. Aminuzzaman, L. H. Tey, S. A. Razali, K. Althubeiti, H. I. Alkhammash, and M. Akhtaruzzaman, "Muntingia calabura leaves mediated green synthesis of CuO nanorods: Exploiting phytochemicals for unique morphology," Materials, vol. 14, no. 21, Art. no. 6379, 2021.

[13] D. Anishya and R. Jain, "Vanillin-mediated green-synthesised silver nanoparticles' characterisation and antimicrobial activity: An in-vitro study," Cureus, vol. 16, no. 1, 2024.

[14] A. L. Valle, A. C. A. Silva, N. O. Dantas, R. Sabino-Silva, F. C. C. Melo, C. S. Moreira, G. S. Oliveira, L. P. Rodrigues, and L. R. Goulart, "Application of ZnO nanocrystals as a surface-enhancer FTIR for glyphosate detection," Nanomaterials, vol. 11, no. 2, Art. no. 509, 2021.

[15] S. Sarkar and R. Das, "PVP capped silver nanocubes assisted removal of glyphosate from water—A photoluminescence study," Journal of Hazardous Materials, vol. 339, pp. 54–62, 2017.